Optical properties and electronic structures of α- and γ-Ce

Joo Yull Rhee
Department of Physics, College of Natural Sciences, Hoseo University, Asan, 336-795 Choongnam, Korea

Xindong Wang, B. N. Harmon, and D. W. Lynch
Ames Laboratory–U.S. Department of Energy and Department of Physics and Astronomy, Iowa State University, Ames, Iowa 50011

(Received 7 June 1993; revised manuscript received 10 February 1994)

The optical properties of metallic α- and γ-Ce were investigated by spectroscopic ellipsometry in the energy range 1.5–5.4 eV. The samples were thin films deposited *in situ* at room temperature and at 25 K for γ- and α-Ce, respectively. The measured conductivities decrease in magnitude as the thickness increases, which can be explained with a microscopic surface roughness model. The optical conductivity increases upon entering the α phase because of the increased number of electrons per unit volume due to the volume collapse. The energy band structures and the optical conductivities were calculated using the linearized-augmented-plane-wave (LAPW) method within density-functional theory, treating both the $4f$ and $5p$ electrons as bandlike. The application of the partial sum rule to angular-momentum-decomposed optical conductivities shows that the $4f$ electron contributions in the measured energy range is small.

I. INTRODUCTION

Metallic Ce exhibits a rich P-T phase diagram and has many peculiar properties.[1] Among these the $\alpha \leftrightarrow \gamma$ isostructural phase transition is one of the most intriguing subjects for both experimentalists and theorists. Both phases have the same fcc structure but the α phase has an approximately 17% smaller volume at 77 K than the γ phase.

Ce is the first element of the rare-earth series where the $4f$ shell starts to fill. It is believed that this single $4f$ electron plays an important role in the isostructural phase transition. After the first discovery of the transition[2] much experimental work, such as magnetic measurements,[3] specific heat measurements,[4–6] positron annihilation,[7] Compton scattering studies,[8] and photoemission[9] were performed to clarify the role of the $4f$ electron in the phase transition.

Several theoretical models were proposed. The Mott transition model[10] allows little difference in the f-electron occupation number for both phases and delocalization of the $4f$ level upon entering the α phase due to the increased $4f$-$4f$ overlap. Because the symmetry does not change, a critical point in the (P,T) phase diagram is expected.

A Kondo volume collapse model using the Anderson impurity Hamiltonian has also been proposed.[11] It was used in the analysis of electron spectroscopy to clarify the $\alpha \leftrightarrow \gamma$ transition using the $1/N$ expansion theory with energy-dependent hybridization calculated in the local-spin-density-functional approximation.[12] The hybridization energy of unoccupied $4f$ states with the conduction bands is much larger than the Kondo energy, but only the Kondo spin fluctuation energy (and entropy) causes the $\alpha \leftrightarrow \gamma$ transition.[13]

Since the first band structure calculation,[14] there have been many self-consistent ones.[15–20] However, the density of states (DOS) using the single-particle approximation does not reproduce the famous two-peak structure in photoemission experiments,[9] where one peak is located at the Fermi level (E_F) and the other is 2 eV below E_F. It is well known that the single-particle approximation for rare earth systems is limited[21] because of the strong localization and consequent correlations of the f-electron states in rare earths. In spite of the problem, the band picture is able to explain some experimental results successfully. For instance, the loss of magnetic moment in the γ phase can be explained by f-sd hybridization, which leads to the delocalization of the $4f$ level upon entering the α phase because the volume collapse causes more overlap of the $4f$ wave functions with those of the valence electrons of neighboring atoms. The increased hybridization between f states and other states with decreased atomic spacing reduces the DOS at the Fermi level and also results in the loss of the magnetic moment.[17]

Glötzel[15] used the self-consistent relativistic linear-muffin-tin-orbital (LMTO) method within the atomic sphere approximation and found 1.2 f electrons in α-Ce, which is consistent with Johansson's idea.[10] Later Podloucky and Glötzel[16] used the same method to reproduce the Compton profile.[8] Pickett *et al.*[17] calculated the band structures of Ce at five different lattice constants using a self-consistent full-potential linearized-augmented-plane-wave (LAPW) method and found that the band structures for both phases are rather similar and the f "bands" become 60% broader upon entering the α phase, which means that the $4f$ state becomes more bandlike in the α phase. Min *et al.*[18] used essentially the same method but treated the $5p$ electrons as valence rather than core

0163-1829/95/51(24)/17390(8)/$06.00

electrons and found the $5p$ band disperses in $\mathbf{k}$ space with a width of almost 200 mRy and has very little influence on the energy position of the $4f$ states. Ionova and Nikolaev[19] used the LAPW method to calculate the band structure of α- and γ-Ce and concluded that the transition was a Mott-type $4f$ localized↔itinerant transition. Eriksson *et al.*[20] calculated band structures for different crystallographic structures under pressure using the LMTO method within the local-density approximation (LDA). The calculations were full potential, all electron, and fully relativistic. They concluded that the delocalization and bonding of $4f$ electrons is important for describing the structural phase transitions in Ce under pressure.

There should be some difference between the optical properties of α- and γ-Ce. However, only a few optical measurements have been made previously on Ce. Wilkins *et al.*[22] measured the reflectance of γ-Ce in the 2–25-μm (0.05–0.62 eV) region and found several absorption peaks. Miyahara *et al.*[23] measured the vacuum ultraviolet absorption spectra for several rare-earth metals, including γ-Ce, from 6 to 40 eV. Neither of these included the visible range and both measured only the γ phase. Pétrakian[24] made normal-incidence reflectivity and transmission measurements on various rare-earth metal thin films including γ-Ce. Although he observed a strong absorption peak at 5.8 eV and attributed it to $M_{2^-} \rightarrow M_{4^+}$ transitions, the vacuum was not good enough ($\sim 10^{-8}$ Torr) to give reasonable data for clean Ce metal. Furthermore, in order to measure transmission, the sample should be thin enough to transmit light partially. A very thin film is likely to be highly strained and, therefore, shows different behavior from that of the bulk. This different behavior is observed in our measurements on very thin films of both phases.

This is the first report of the optical properties of both phases of Ce metal in the infrared-visible-ultraviolet region. We measured the dielectric functions of α- and γ-Ce at various temperatures with various film thicknesses using spectroscopic ellipsometry. We observed few structures in the measured energy range and found some thickness dependence. The change in magnitude of the dielectric functions in going from the γ to the α phase could be explained by the volume collapse, and the slight change of the shape of the spectra indicates a small change of the oscillator strengths. In order to understand this better, we calculated the band structure and the optical conductivities for both phases using the LAPW method. While a single-particle model, such as the band theory we use, is not expected to treat the $4f$ excitation spectrum correctly, a comparison between the experimental results and the results of a careful band calculation is the first step in assessing the presence and importance of correlated, many-body effects. The results of the calculation show that there are some oscillator strength changes for the valence electrons and changes in f-sd valence band hybridization, and that the $4f$ electron plays no significant role in the difference between the optical conductivities of γ- and α-Ce in the measured energy range.

In Sec. II, we describe the experiments briefly. In Sec. III, the calculational procedure is presented. In Sec. IV, the results of measurements and calculations are given and discussed. Section V concludes this paper.

II. EXPERIMENT

The experimental setup and its alignment, initialization and calibration procedure, and the sample preparation procedures are described in detail elsewhere.[25] Therefore, we will give only a brief description here.

A. Sample preparation

The samples were thin films evaporated *in situ*. The chamber pressure was kept below 2×10^{-9} Torr during evaporation and below 2×10^{-10} Torr during measurements. Therefore, oxidation can be neglected because sample preparation and measurements were finished in less than 1 h. We deposited thin films repeatedly on top of previously deposited films to investigate the thickness dependence. A high purity electropolished piece of bulk Ce prepared by the Ames Laboratory was used as an evaporant source in a tungsten basket. γ-Ce was deposited on room temperature substrates, α-Ce on substrates at 25 K. The sample holder and the substrates were cooled with a closed-cycle helium refrigerator. α-Ce prepared in this way contains a negligible amount of γ-Ce.[26] The substrate was an optically polished sapphire disk.

B. Ellipsometer

A rotating-analyzer ellipsometer[27–29] was built. We used a high-pressure 75-W Xe-arc lamp as a light source, a high-intensity $\frac{1}{4}$-m grating monochromator, and a 5-cm-diameter end-on photomultiplier (PM) tube with an extended S-20 response as a detector. A five-phase stepping motor with an angular resolution of 0.18°/step was used to rotate the polarizer and a two-phase hybrid stepping motor with an angular resolution of 1.8°/step was used for faster rotation of the analyzer. A mechanical shutter was placed between the monochromator and the polarizer for corrections for the dark current of the PM tube and for stray light.

We used a pair of crystal quartz Rochon prisms for both polarizer and analyzer. Although a quartz Rochon prism has a better spectral transmittance in both the IR and UV, and a smaller angle of deviation of the centrally transmitted light beam than a calcite one, it is optically active. The optical activity means that two different things happen at the same time when light travels through such a medium;[30] (1) if linearly polarized light passes through an optically active medium, the direction of polarization rotates and the amount of rotation is proportional to the distance traveled and (2) the linearly polarized light becomes slightly elliptically polarized when it propagates in any direction except 56°10′ from the optic axis of quartz. The first problem can be solved by the proper choice of the direction of the quartz

Rochon prism.[28] For the second problem, Aspnes developed a first-order calibration procedure.[28,29] We followed the same procedure but with a slightly different method for the determination of the initial angles of the polarizer and the analyzer. Aspnes used the first-order correction to find the initial angles of the polarizer and the analyzer but we found them by iteration.

Because Ce is highly reactive with oxygen, the sample was prepared inside the UHV measurement chamber. The effect of the fused silica window was checked and found to be negligible.[25]

III. BAND STRUCTURE CALCULATIONS

Both phases of Ce have the same fcc structure but different lattice constants; for γ-Ce, a=9.7529 a.u. (5.161 Å) and for α-Ce, a=9.1660 a.u. (4.850 Å) were used.[1] We treated both the f electron and the $5p$ electrons as band electrons.[18] We calculated the self-consistent band structure using a scalar-relativistic version of the LAPW method.[31] The spin-orbit interaction was included in the self-consistent calculation in such a way that the spin-orbit Hamiltonian was diagonalized after the scalar-relativistic bands and wave functions had been obtained. The muffin-tin radius was chosen so that each sphere almost touches the neighboring sphere; for γ-Ce R_{MT}= 3.385 a.u. (1.791 Å) and for α-Ce R_{MT}= 3.180 a.u. (1.683 Å). The potential was spherically symmetric inside the muffin tin and constant outside. The LDA of Hedin and Lundqvist[32] to the density-functional formalism was used to include the exchange-correlation contribution to the potential.

A 60–80 LAPW basis function set, depending on the $\mathbf{k}$ point, was used, which satisfies $K_{\max}R_{\mathrm{MT}} = 9.0$ for the muffin-tin radius R_{MT}. For the self-consistent iterations, the energy eigenvalues at 60 $\mathbf{k}$ points in the irreducible Brillouin zone [(IBZ)=$\frac{1}{48}$ of the BZ)] were calculated.

Once the self-consistent potential and charge were obtained, we calculated the energy eigenvalues at the four corners and the centers of 1536 tetrahedra in the IBZ for the calculation of the optical conductivity. The optical conductivity was calculated using the linear-energy-tetrahedron method.[33] The optical conductivity is given as

$$\sigma = \frac{\pi e^2}{3m^2\omega}\sum_{f,i} \times \int_{\mathrm{BZ}} d^3k \frac{2}{(2\pi)^3} |\mathbf{P}_{fi}|^2 \, \delta\left[E_f(\mathbf{k}) - E_i(\mathbf{k}) - \hbar\omega\right], \quad (1)$$

where

$$\mathbf{P}_{fi} = \frac{\hbar}{i} \langle f | \nabla | i \rangle , \quad (2)$$

where m and e are the electronic mass and charge, respectively, $\hbar\omega$ is the energy of the incident photon, $E_i(\mathbf{k})$ and $E_f(\mathbf{k})$ are the energies of the initial and final states, respectively, and $\mathbf{k}$ is the wave vector inside the BZ where the transition $E_i(\mathbf{k}) \rightarrow E_f(\mathbf{k})$ occurs. Of course, the initial (final) state, $|i\rangle$ ($|f\rangle$) is occupied (empty). Here we assume only direct transitions as usual. The energy eigenvalues at the four corners of 1536 tetrahedra were used for the calculation of the DOS and joint DOS, $\delta\left[E_f(\mathbf{k}) - E_i(\mathbf{k}) - \hbar\omega\right]$, and those of the centers were used for the calculation of energy differences $[E_f(\mathbf{k}) - E_i(\mathbf{k})]$ in Eq. (1). The wave functions at the centers of the tetrahedra were calculated and used for the calculation of the dipole matrix elements, Eq. (2). To partially simulate the imaginary part of the quasiparticle self-energy, the calculated optical conductivity was convoluted with an energy-dependent Lorentzian broadening function of width $\Gamma(E) = AE^2/\mathrm{eV}$ where $E = [E_f(\mathbf{k}) - E_i(\mathbf{k})]$, in eV. $\Gamma(E)$ was set to 2 eV if AE^2/eV was larger than 2 eV. A was set to 0.1 and 0.15 for the γ and α phase, respectively, in order to reflect roughly the increased quasiparticle damping caused by the increased density.

IV. RESULTS AND DISCUSSION

The measured dielectric functions were dependent on sample thickness. Figures 1 and 2 show the optical conductivities of γ- and α-Ce, respectively, with various thicknesses. As shown, the optical conductivity decreases as thickness increases.

It is generally believed that the sample with the smoother surface has the larger optical conductivity. Aspnes *et al.*[34] made gold thin films on cleaved NaCl surfaces at various temperatures and found that the film made at liquid nitrogen temperature showed the smallest imaginary part of the dielectric function in the interband transition region and it was full of voids and defects. Based on this, we can conclude that our samples become rougher as the thickness increases because the optical conductivity decreases. To check this point we applied a microscopic surface roughness model using the Bruggeman effective medium approximation (BEMA),[36]

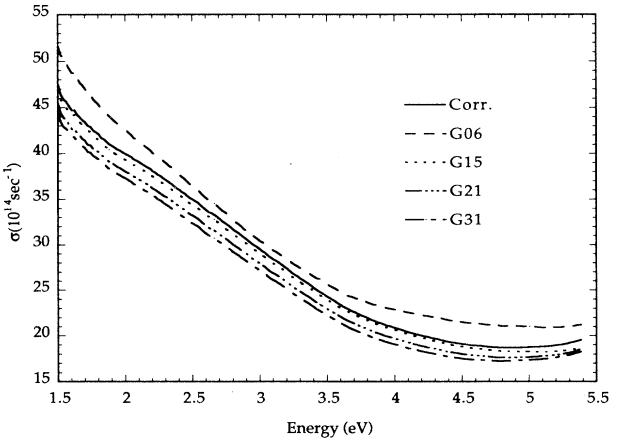

FIG. 1. Optical conductivities of γ-Ce of various thicknesses. See Table I for sample designation. Note that the zero of the optical conductivity is suppressed.

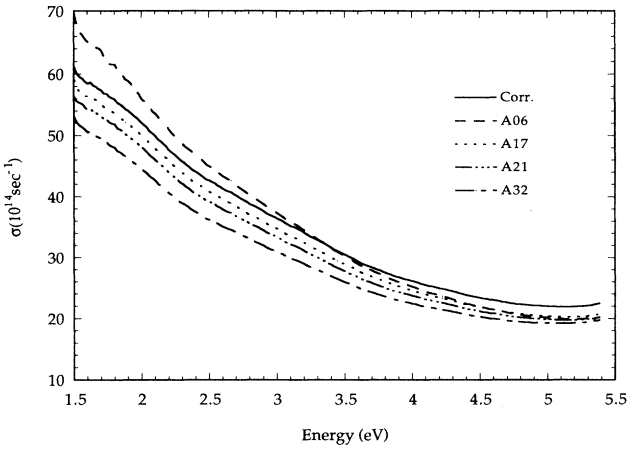

FIG. 2. The same as Fig. 1 except for α-Ce.

which was shown to be an appropriate model by Aspnes *et al.*[35] We used a three-phase model, instead of a two-phase model, in the analysis where the rough overlayer was modeled as a mixture of voids and Ce. The BEMA gives the complex dielectric function of the overlayer from

$$\sum_i v_i \frac{\tilde{\epsilon}_i - \langle\tilde{\epsilon}\rangle}{\tilde{\epsilon}_i + 2\langle\tilde{\epsilon}\rangle} = 0, \tag{3}$$

where $\langle\tilde{\epsilon}\rangle$ is the measured dielectric function and $\tilde{\epsilon}_i$ and v_i are the dielectric function and the volume fraction of the ith medium. The v_i's satisfy the relationship

$$1 = \sum_i v_i. \tag{4}$$

Here i=void and Ce. As we can see in Figs. 1 and 2, the thinnest samples ($G06$ for the γ phase and $A06$ for the α phase) have the largest optical conductivities; however, the magnitudes are rather large compared to the others and the spectral shapes are appreciably different from the others. The thinnest sample might be severely strained and, therefore, show a very different behavior from the other, thicker samples. Therefore, we did not include these samples in the fitting procedure. We fit the other three thicker samples with six parameters that are adjusted in the fitting procedure. Each sample has two parameters, the thickness of the overlayer d_o and the void fractions v_o.

The measured complex reflectance ratio for the three-phase model is given by[37]

$$\tilde{\rho} = \left\{\frac{\tilde{Z}\tilde{r}_{p,ob} + \tilde{r}_{p,ao}}{\tilde{Z}\tilde{r}_{p,ob}\tilde{r}_{p,ao} + 1}\right\} \Big/ \left\{\frac{\tilde{Z}\tilde{r}_{s,ob} + \tilde{r}_{s,ao}}{\tilde{Z}\tilde{r}_{s,ob}\tilde{r}_{s,ao} + 1}\right\}, \tag{5}$$

where

$$\tilde{r}_{p,ij} = \frac{\tilde{\epsilon}_j\sqrt{\tilde{\epsilon}_i - \sin^2\phi} - \tilde{\epsilon}_i\sqrt{\tilde{\epsilon}_j - \sin^2\phi}}{\tilde{\epsilon}_j\sqrt{\tilde{\epsilon}_i - \sin^2\phi} + \tilde{\epsilon}_i\sqrt{\tilde{\epsilon}_j - \sin^2\phi}}, \tag{6}$$

$$\tilde{r}_{s,ij} = \frac{\sqrt{\tilde{\epsilon}_i - \sin^2\phi} - \sqrt{\tilde{\epsilon}_j - \sin^2\phi}}{\sqrt{\tilde{\epsilon}_i - \sin^2\phi} + \sqrt{\tilde{\epsilon}_j - \sin^2\phi}}, \tag{7}$$

and

$$\tilde{Z} = \exp\left(4\pi i\sqrt{\tilde{\epsilon}_o - \sin^2\phi}\frac{d_o}{\lambda}\right). \tag{8}$$

The subscripts a, o, and b in Eqs. (5)–(8) stand for the ambient (vacuum), the overlayer, and the bulk, and subscripts p and s in Eqs. (6) and (7) for p and s polarization, respectively. The subscripts ij in Eqs. (6) and (7) stand for either ao or ob. Initially we estimate the six parameters. By substituting them into Eq. (5) and comparing with three measured complex reflectance ratios, $\tilde{\rho}$, we can find the dielectric functions of the bulk for the three samples. To find the dielectric functions of the overlayer we used Eq. (3). If we correctly guessed the six parameters, the calculated bulk dielectric functions for three samples should be equal to each other. Furthermore, those six parameters should be independent of photon energy. In the fitting procedure,[38] we found the six parameters by minimizing

$$s \equiv \sum_{j=1}^{j_{\max}} \{|\tilde{\epsilon}_1(E_j) - \tilde{\epsilon}_2(E_j)| + |\tilde{\epsilon}_2(E_j) - \tilde{\epsilon}_3(E_j)|\}^2, \tag{9}$$

where the subscripts 1, 2, and 3 refer to the three samples, respectively. $j_{\max}$ is the number of data points and E_j is the energy of the jth measurement. Since we measured from 1.505 eV to 5.385 eV with an energy step of 0.02 eV, $j_{\max} = 195$. The numerical values of $\sqrt{s/j_{\max}}$ are 0.080 for the γ phase and 0.176 for the α phase.

The corrected optical conductivity of each phase is included in Figs. 1 and 2 as a solid line. There are some differences between the corrected optical conductivity and the as-measured optical conductivity of the second thinnest sample. As summarized in Table I, the fitting results show that both the void fraction and the overlayer thickness increase as the sample thickness increases except for the case of $G31$, the thickest γ-Ce sample, which has smaller overlayer thickness but much higher void fraction than $G21$.

The grain size normal to the substrate is essentially the same as the film thickness, provided that the film thickness is less than 1 μm.[39] The surface roughness depends on the statistical process of nucleation and growth and

TABLE I. Three-phase fitting results.

Sample	Thickness (Å)	d_o (Å)	v_o (%)
G06	140		
G15	333	16.6	5.47
G21	477	59.1	5.93
G31	705	33.8	12.55
A06	119		
A17	334	34.2	7.04
A21	411	81.2	7.17
A32	625	112.7	10.98

on the adatom surface mobility. A large anisotropy of the surface energy and the presence of faceted roughness on the substrate each enhance the surface roughness.[40] Since the crystallographic and topographic orientations of the grains are random, grain boundaries and various point and line defects are formed when two grains touch each other in the agglomeration stage. This randomness of the orientations of grains causes surface roughness and the surface roughness is enhanced by, for instance, oblique deposition.[40] The further incoming evaporant atoms are attached epitaxially to each grain. The epitaxially grown grains make the film rougher because of the randomness of the crystallographic and topographic orientation of the grains. Therefore, the film becomes rougher as the film grows. This agrees well with our fitting results.

At low substrate temperatures, the surface becomes rougher than at high substrate temperatures because of low adatom surface mobility. The roughness is proportional to the square root of thickness.[40] Our fitting results do not follow this rule. However α-Ce has a thicker overlayer than γ-Ce, which is consistent with the low adatom surface mobility because the α-Ce samples were deposited at 25 K.

Since our measurements do not extend below 1.5 eV, we are unable to assess the Drude part of the conductivity. We did measure the spectra for the γ phase at room temperature and at 120 K (where the dc conductivity increases by 12%) in order to ascertain any temperature-dependent changes in the low-energy part of the spectra that might behave like a Drude contribution. We were unable to detect any changes. It is possible, however, that the much higher dc conductivity for the α phase would give rise to some Drude contribution extending into the lower-energy part of our measured spectrum; although with the lower scattering rates (larger relaxation time) at low temperature, the Drude contributions should fall off fairly rapidly with energy and would not be expected to contribute appreciably above 1.5 eV.

The corrected optical conductivities of the two phases show little difference in spectral shape, but show a slight convex upward (downward) shape in the energy range below 2.5 eV for the α (γ) phase (see Fig. 3). The major difference obvious in Fig. 3 is that α-Ce has a larger optical conductivity throughout the measured energy range.

The optical conductivity of α-Ce is expected to be different from that of γ-Ce for two reasons if the temperature dependence of the Drude term is neglected. The first is the volume collapse upon entering the α phase. Since the α phase has a larger electron concentration because of reduced lattice spacing and the optical conductivity scales with this quantity [see Eq. (10) and (11)], other factors remaining the same, α-Ce may be expected to have the larger optical conductivity by about 17%. The second reason is related, since the volume collapse also causes increased wave function overlap (hybridization) and changes the oscillator strengths and the energy differences between the states for which electronic transitions occur. This may increase the optical conductivity if the change in the energy bands pulls other transitions into the measured energy range, or increase the oscillator strength for transition already in this range. Many

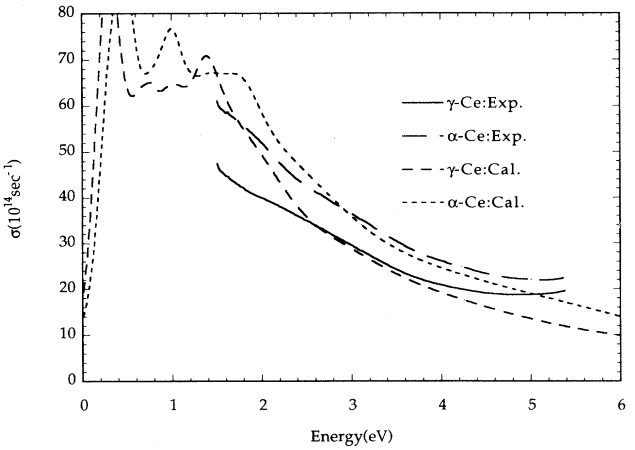

FIG. 3. Optical conductivities of α- and γ-Ce. Both experimental (corrected) and theoretical results are shown.

band structure calculations[15–19] showed that both phases have rather similar band structures and suggest the $4f$ localized $\rightarrow$ itinerant transition occurs upon entering the α phase due to the increased hybridization. Experiments as well as the calculations show that the $4f$ occupation number is relatively unchanged upon entering the α phase; however, the $4f$ bands become wider.[17]

To further assess the effects of the volume and hybridization changes, we applied the sum rule

$$\int_0^\infty \sigma(\omega)d\omega = \frac{1}{8}\omega_p^2, \tag{10}$$

where the plasma frequency ω_p is

$$\omega_p^2 = \frac{4\pi n e^2}{m}, \tag{11}$$

and where n is the electronic density. Since it is impossible to measure the dielectric functions in the whole energy range from 0 to ∞, we have to apply the partial sum rule

$$\int_{\omega_i}^{\omega_f} \sigma(\omega)d\omega = \frac{\pi e^2}{2mV_c} n_{\text{eff}}, \tag{12}$$

where ω_i and ω_f are the lower and upper bounds of the measured spectrum and V_c is the volume occupied by a single atom. Here we interpret n_{eff} as the number of electrons per atom participating in optical transitions within the measured energy range due to the absorption of photons.

The difference in n_{eff} between the two phases is very small (Table II). This is a somewhat surprising result because the spectral line shape difference (albeit small) in the energy range below 2.5 eV indicates a change in the oscillator strength, possibly leading to some difference in n_{eff}. Since σ for the α phase is convex upward and that of the γ phase is convex downward, the oscillator strength in this energy range increases upon entering the α phase.

TABLE II. Partial sum rule in the 1.5–5.4-eV range for angular-momentum-decomposed calculated optical conductivity.

n_{eff} (elec./atom)	Total[a]	$s \to p$	$p \to d$	$d \to f$	$f \to g$	Exp.
γ-Ce	1.423	0.276	0.073	0.186	0.023	1.414
α-Ce	1.487	0.221	0.085	0.157	0.035	1.464
n_{eff}(elec./atom)	MTO[b]	$p \to s$	$d \to p$	$f \to d$	$g \to f$	Sum[c]
γ-Ce	0.331	0.003	0.369	0.008	0.002	1.271
α-Ce	0.349	0.004	0.440	0.011	0.005	1.306

[a]See text.
[b]Outside the muffin-tin sphere.
[c]See text.

The experimental data show that n_{eff} is 0.05 larger in α-Ce than in γ-Ce. It is expected that the $4f$ electrons give little contribution to the optical conductivity in the measured energy range because of the large centrifugal potential,[41] which leads to poor overlap of initial and final states. On the other hand, Kim *et al.*[42] recently found some oscillator strength for the $4f$ electron in $CeSn_3$ in the energy range of 1.5–4.35 eV. However there were some errors in both calculations and measurements. Both were repeated[43] and showed little $4f$-electron contribution. On the other hand, there were large sum rule differences between CeSb and LaSb (Ref. 44) and between CeB_6 and LaB_6.[45] For CeB_6 and LaB_6, however, different measurements[46] showed little difference. To assess whether the differences in the measured optical conductivities for γ- and α-Ce come from $4f$ electrons or not, the band structures and the optical conductivities were calculated.

We carried out band structure calculations as described in Sec. III. The overall shapes of the calculated band structures are very similar to others.[16–19] As expected, the $4f$ bands do not disperse very much with wave vector $\mathbf{k}$. There is little difference in the band structures between the two phases but α-Ce has wider f bands. As mentioned above, we treated the $5p$ electrons as band electrons. We found that the $5p$ states have a width of approximately 200 mRy in γ-Ce and disperse with wave vector $\mathbf{k}$, which is similar to the results of Ref. 18. This dispersion might be measurable by angle-resolved photoemission, although we would expect the $5p$ states to be so localized that their photoemission spectrum will be dominated by atomiclike multiplet fine structure,[47] and smeared out by lifetime broadening.

The calculated and measured optical conductivities are drawn together in Fig. 3. The calculated optical conductivities below 2 eV show rich structures and appreciable difference between the two phases, but are almost structureless above 2 eV. The calculation also reproduces the subtle convex upward (downward) shape in the 1.5–2.5-eV range for the α (γ) phase similar to the measured ones.

We performed an angular-momentum decomposition of the optical conductivity inside the muffin-tin sphere and applied the partial sum rule, Eq. (12), in the measured energy range to clarify the role of $4f$ electrons in the optical properties. The results are summarized in Table II. "Total" means the use of the partial sum rule after the calculation of the optical conductivity and "sum" means the sum of the partial sum rule for the angular-momentum-decomposed optical conductivities. The decomposed optical matrix elements are complex numbers and the total optical matrix element is the sum of the decomposed optical matrix elements. Since the optical matrix elements then are absolute squared, there can be interference terms among the various angular-momentum contributions in the "total" (corrected) case, but not in the "sum" case. These were found to cause rather small effects in the energy range of the measurements. The existence of both constructive and destructive interference in this spectral range may partially cancel and make the effect small for the integral of the conductivity. However, the interference terms were found to be very important at energies below 1.5 eV.

As given in Table II, the main changes in going from γ- to α-Ce are an increase in the $d \to p$ contributions and a 18% decrease in the $s \to p$ contributions. We can associate some of these changes as arising from an $\sim$18% drop in the amount of s character inside the muffin-tin sphere and an 8% increase in d character (see Table IV of Ref. 17). In spite of a 10% increase in the amount of f character in going from γ- to α-Ce, the $f \to d$ contributions remain very small, while the $d \to f$ contributions are decreased about 6.1%, despite the increased d occupation.

We should mention that the $d \to f$ contributions that we calculated are likely to be incorrectly positioned. This is because such transitions shift an electron with d-like character to one with f character, creating an increase in the $4f$ occupation. The Coulomb repulsion among the electrons in the $4f$ shell is very large, which has the effect of pushing the energy of such transitions $\sim$ 6–7 eV (Ref. 48) higher (for pure f final states) than what our single-particle band calculations would predict. The calculations show that the valence electron contributions, except for $s \to p$ transitions, increase upon entering the α phase (see Table II) with a net theoretical n_{eff} change of 0.064 electrons. Although the experiment showed a small difference in n_{eff} (0.05 electrons per atom), the experimental value of n_{eff} for the α phase is considered an underestimate of the actual value due to the suppressed Drude contribution. Thus, the agreement between experiment and calculation is not unreasonable. The $d \to f$ transitions contribute about 1/6 electrons per unit cell to n_{eff} and decrease by 0.03 electrons per atom upon en-

tering the α phase, thus, n_{eff} for $d \rightarrow f$ transitions is not negligibly small; however, this is likely to be inaccurate because of the large $f - f$ Coulomb repulsion, as mentioned above. In an attempt to take this into account, we arbitrarily added an energy, proportional to the difference in f-electron occupation number times an effective Coulomb repulsion, U, of about 6 eV, to the final state energy in the calculation of the optical conductivity. However, this procedure did not produce a spectrum closer to the experimental results. This may be due to the fact that if the energy eigenvalue of the final state changes then its wave function also changes and, hence, the optical matrix element changes. It is more probable that atomiclike correlation involving the $4f$ electrons are important. Therefore, the inclusion of the effects of the large $f-f$ Coulomb repulsion needs a more sophisticated treatment. Liechtenstein *et al.*[49] applied the so-called "LDA+U" method to CeSb. They reproduced the optical conductivity and magneto-optic spectra successfully. The same method was applied to Ce, but it failed to converge in the course of a self-consistent calculation.[50]

Recently, Weschke *et al.*[51] found that the surface of the α-Ce is γ-like. We believe that this surface effect is negligible for our measurements on the α phase because the thickness of the surface layer is of the order of 1 Å but the depth of the optical probe is of the order of a few hundred Å. Therefore, we neglected the effect of a γ-like overlayer on the surface of the α phase.

Since the increased $4f$ band width and smaller lattice constant for α-Ce lead to an increase in hybridization of the $4f$ electrons with the other conduction bands, we expected we might see some noticeable increase in the $4f$ contributions to the optical conductivity. Instead we found the $4f \rightarrow 5d$ contributions remain very small, and the $5d \rightarrow 4f$ contributions decrease in spite of the increase in the occupation of the d bands. Although we expected some changes in spectral shape because of the difference in the lattice spacings and, in turn, the difference in the $4f$-sd valence band hybridization, the experiments show little change. Therefore, we calculated the difference in the optical conductivity times unit cell volume between the two phases, $(\sigma V_c)_\alpha - (\sigma V_c)_\gamma$, and plotted it in Fig. 4 together with the calculated one. It shows two positive peaks (at 1.7 and 3.8 eV) and one negative peak (at 2.6 eV). The positive peak at 1.7 eV is fairly sharp, which reflects the difference already seen in Fig. 3, and the other two are very broad. The overall shapes of experimental and calculated spectrum are similar if the theoretical spectra is scaled to lower energies (a common observation usually ascribed to self-energy effects.[52]) The positive peak at 2.6 eV would correspond to the experimental one at 1.7 eV, the broad positive peak at 5 eV to the experimental one at 3.8 eV, and the negative peak at 3.3 eV, to the experimental one at 2.7 eV. These results suggest that the self-energy corrections may be important for the calculated optical conductivity of metallic Ce. Figure 4 suggests that there is some oscillator strength change in the measured energy range and the change is responsible for the difference in n_{eff}. The similarity between the measured and the calculated differences means that the band structure calculation is a good starting point to understand the optical properties of Ce (at least in the 1.5–5.4-eV energy range).

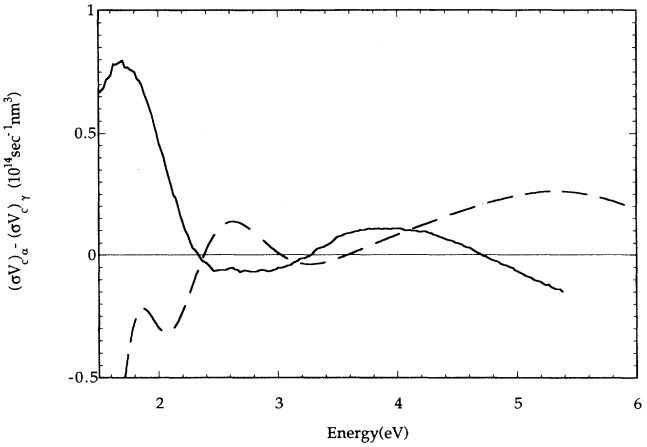

FIG. 4. The difference between the optical conductivity times unit cell volume of α-Ce and γ-Ce. Solid line, experimental; dashed line, calculated.

V. CONCLUSIONS AND SUMMARY

We have measured the optical conductivity for both α- and γ-Ce by spectroscopic ellipsometry. The measured dielectric functions decrease monotonically as the sample thickness increases, an indication of increased surface roughening. A microscopic surface roughness model with BEMA was applied and we found that the thicker the sample, the rougher the surface. Both overlayer thickness and void fraction increase as the sample thickness increases. Using a three-phase model, we can estimate the bulk value of the optical conductivity.

The overall increase of the magnitude of the measured optical conductivity upon entering the α phase is due to the volume collapse. The results of the application of the partial sum rule showed that there is some change in n_{eff}. The calculations of the band structures and the optical conductivities showed that there may be some small changes for contributions from both f electron and valence electrons and that the $4f$ electron does not play a significant role in the change of the optical conductivities in the 1.5–5.4-eV range. The calculated change in the total n_{eff} was about +0.064 electrons/atom upon entering the α phase. The difference in change in n_{eff} between experiment and calculation is not unreasonable. The difference, $(\sigma V_c)_\alpha - (\sigma V_c)_\gamma$, indicates that there is some oscillator strength change, which is responsible for the change in n_{eff}.

The measured spectra showed little structure but the calculations showed rich structures outside the measured energy range, especially below 2 eV (a region where band theory is especially suspect). Therefore, optical measurements below 1.5 eV and above 6 eV may further clarify the role of $4f$ electron in the optical properties of Ce. The

low-energy measurement is quite difficult because sample preparation and all measurements should be done *in situ* for Ce and the onset of interband transition is expected to be at very low energy (see Fig. 3 and Ref. 22). However, recent developments in IR ellipsometry may enable these measurements.[53]

ACKNOWLEDGMENTS

The Ames Laboratory is operated for the U.S. Department of Energy by Iowa State University under Contract No. W-7405-Eng-82.

[1] D. C. Koskenmaki and K. A. Gschneidner, Jr., in *Handbook on the Physics and Chemistry of Rare Earths*, edited by K. A. Gschneidner, Jr. and L. R. Eyring (North-Holland, Amsterdam, 1978), Vol. 1, Chap. 4.
[2] P. W. Bridgeman, Proc. Am. Acad. Arts Sci. **62**, 207 (1927).
[3] M. R. MacPherson, G. E. Everett, D. Wolleben, and B. Maple, Phys. Rev. Lett. **26**, 20 (1971).
[4] N. E. Phillips, J. C. Ho, and T. F. Smith, Phys. Lett. **27A**, 49 (1968).
[5] N. T. Panousis and K. A. Gschneidner, Jr., Solid State Commun. **8**, 1779 (1970).
[6] D. C. Koskimaki and K. A. Gschneidner, Jr., Phys. Rev. B **11**, 4463 (1975).
[7] D. R. Gustafson, J. D. McNutt, and L. O. Roelling, Phys. Rev. **183**, 435 (1969).
[8] U. Kornstädt, R. Lässer, and B. Lengeler, Phys. Rev. B **21**, 1898 (1980).
[9] D. W. Lynch and J. H. Weaver, in *Handbook on the Physics and Chemistry of Rare Earths* (Ref. 1), Vol. 10, Chap. 66, and references therein.
[10] B. Johansson, Philos. Mag. **30**, 469 (1977).
[11] J. W. Allen and R. M. Martin, Phys. Rev. Lett. **49**, 1106 (1982).
[12] L. Z. Liu and J. W. Allen, Phys. Rev. B **45**, 8934 (1992).
[13] J. W. Allen and L. Z. Liu, Phys. Rev. B **46**, 5047 (1992).
[14] E. A. Kmekto and H. H. Hill, in *Plutonium 1970 and other Actinides*, edited by W. N. Miner (AIME, New York, 1970), p. 233.
[15] D. Glötzel, J. Phys. F **8**, L163 (1978).
[16] R. Podloucky and D. Glötzel, Phys. Rev. B **27**, 3390 (1982).
[17] W. E. Pickett, A. J. Freeman, and D. D. Koelling, Phys. Rev. B **23**, 1266 (1980).
[18] B. I. Min, H. J. F. Jensen, T. Oguchi, and A. J. Freeman, Phys. Rev. B **34**, 369 (1986).
[19] G. V. Ionova and A. V. Nikolaev, Phys. Status Solidi B **162**, 451 (1990).
[20] O. Eriksson, J. M. Wills, and A. M. Boring, Phys. Rev. B **46**, 12 981 (1992).
[21] B. N. Harmon, J. Phys. C **5**, 65 (1979)
[22] J. F. Wilkins, J. G. Clark, and T. E. Leinhardt, Bull. Am. Phys. Soc. **7**, 579 (1962).
[23] T. Miyahara, H. Ichii, H. Ohkuma, and S. Yamaguchi, J. Phys. Soc. Jpn. **51**, 1834 (1982).
[24] J. P. Pétrakian, J. Opt. Soc. Am. **62**, 401 (1972).
[25] J. Y. Rhee, Ph.D. thesis, Iowa State University, 1992.
[26] D. M. Wieliczka, J. H. Weaver, D. W. Lynch, and C. G. Olson, Phys. Rev. B **26**, 7056 (1982).
[27] D. E. Aspnes, Opt. Commun. **8**, 222 (1973).
[28] D. E. Aspnes, J. Opt. Soc. Am. **64**, 812 (1974).
[29] D. E. Aspnes, J. Opt. Soc. Am. **65**, 1274 (1975).
[30] J. F. Nye, *Physical Properties of Crystals* (Oxford University Press, London, 1985), p. 260ff.
[31] D. D. Koelling and B. N. Harmon, J. Phys. C **10**, 3170 (1977).
[32] L. Hedin and B. I. Lundqvist, J. Phys. C **4**, 2064 (1971).
[33] O. Jepsen and O. K. Anderson, Solid State Commun. **9**, 1763 (1971).
[34] D. E. Aspnes, E. Kinsborn, and D. D. Bacon, Phys. Rev. B **21**, 3290 (1980).
[35] D. A. G. Bruggeman, Ann. Phys. (Leipzig) **24**, 636 (1935).
[36] D. E. Aspnes, J. B. Theeten, and F. Hottier, Phys. Rev. B **20**, 3292 (1979).
[37] D. E. Aspnes, in *Optical Properties of Solids-New Developments*, edited by B. O. Seraphin (North-Holland, Amsterdam, 1976), Chap. 15.
[38] We used the IMSL subroutine DBCLSF for fitting.
[39] K. L. Chopra and I. Kaur, *Thin Film Device Applications* (Plenum, New York, 1983).
[40] K. L. Chopra, *Thin Film Phenomena* (McGraw-Hill, New York, 1969).
[41] U. Fano and J. W. Cooper, Rev. Mod. Phys. **40**, 441 (1968).
[42] K. J. Kim, B. N. Harmon, D. W. Lynch, and D. D. Koelling, Phys. Rev. B **44**, 8526 (1991).
[43] J. Y. Rhee, B. N. Harmon, and D. W. Lynch, Phys. Rev. B **50**, 5693 (1994).
[44] Y. S. Kwon, M. Takeshige, T. Suzuki, and T. Kasuya, Physica B **163**, 328 (1990).
[45] P. A. M. van der Heide, H. W. ten Cate, L. M. ten Dam, R. A. de Groot, and A. R. de Vroomen, J. Phys. F **16**, 1617 (1986).
[46] S. Kimura, T. Nanba, S. Kunii, and T. Kasuya, J. Phys. Soc. Jpn. **59**, 3388 (1990).
[47] B. T. Thole, X. D. Wang, B. N. Harmon, D. Li, and P. A. Dowben, Phys. Rev. B **47**, 9098 (1993).
[48] Y. Baer, H. R. Ott, J. C. Fuggle, and L. E. De Long, Phys. Rev. B **24**, 5384 (1981).
[49] A. I. Liechtenstein, V. P. Antropov, and B. N. Harmon, Phys. Rev. B **49**, 10 770 (1994).
[50] V. P. Antropov (private communication).
[51] E. Weschke, C. Laubschat, T. Simmons, M. Domke, O. Strebel, and G. Kaindl, Phys. Rev. B **44**, 8304 (1991).
[52] K. J. Kim, B. N. Harmon, and D. W. Lynch, Phys. Rev. B **43**, 1948 (1990).
[53] A. Röseler, *Infrared Spectroscopic Ellipsometry* (Akademie-Verlag, Berlin, 1988).